

Study of circular geodesics and shadow of rotating charged black hole surrounded by perfect fluid dark matter immersed in plasma

Anish Das^{*a}, Ashis Saha^{†b}, Sunandan Gangopadhyay^{‡c}

^{a,c}*Department of Theoretical Sciences, S.N. Bose National Centre for Basic Sciences, JD Block, Sector-III, Salt Lake, Kolkata 700106, India*

^b*Department of Physics, University of Kalyani, Kalyani 741235, India*

Abstract

In this work, we consider a rotating charged black hole surrounded by perfect fluid dark matter [1]. We consider the system to be immersed in non-magnetic, pressureless plasma. We then evaluate the null geodesics in order to study the co-rotating and counter rotating photon orbits. Later we analyse the null geodesics further, to calculate the celestial coordinates (α, β) . The celestial coordinates are used to determine the shadow radius (R_s). After that we observe and analyse the effects of black hole spacetime, perfect fluid dark matter and plasma parameters (a, Q, χ, k) on the black hole shadow in detail. Finally, we study the effect of plasma distribution on the effective potential (V_{eff}) of the black hole spacetime as encountered by the photons.

1 Introduction

Recent advancement in observational astrophysics paved the way for the release of the first image of supermassive black hole [2]. Black holes are one of the most intriguing predictions of general theory of relativity. It is predicted that supermassive black holes form the core of almost all the galaxies in the universe. The image released by the *EHT* group depict the supermassive black hole residing at the center of Messier 87 galaxy [2]. Theoretical analysis of the formation of the image of black holes (*black hole shadow*) started with the works of Synge [3] who demonstrated the shadow of spherically symmetric black hole. Later, Luminet [4] studied the shadow of black hole surrounded by accretion disks. Shadows are dark disks formed by light coming from a background source when a black hole lies between the source and observer. Due to gravitational lensing, light from the source bends around the black hole and makes its way out to the observer, imaging the black hole boundary. The study for Kerr and Kerr-Newman black holes were carried out in [5],[6] and [7]. With improvement in observational data from time to time, black hole shadows were studied in GR [8]-[31], modified gravity theory [32]-[38] as well as higher dimensional gravity theories [39]-[41]. Besides, black hole shadow analysis were carried out considering expanding universe [42],[43].

General relativity has impressed us time and again by its impeccable predictions. But it still lacks to incorporate two of the major constituents of the universe- dark energy and dark matter. These two comprise nearly 95-96 % of the total mass-energy content of the universe. Studies were conducted using dark energy models comprising of cosmological constant (Λ) [44],[45], quintessence [46],[47], etc. But here in this case we want to study black hole shadow neglecting dark energy and considering only dark matter (*DM*). Dark matter are non-baryonic and non-luminous in nature comprising about 27 % of the mass-energy content of the universe. Many observations such as galaxy rotation curves [48] and dynamical motion of galaxy clusters [49] predicted their existence. Many possible candidates for dark matter were proposed, such as

*anishdasslg@gmail.com, anishdas1995@bose.res.in

†sahaashis0007@gmail.com, ashisphys18@klyuniv.ac.in

‡sunandan.gangopadhyay@gmail.com, sunandan.gangopadhyay@bose.res.in

WIMPs, axions, primordial black holes, neutralinos, etc. But none of the models have correctly matched the observations. In view of all these, we wish to work in a model named perfect fluid dark matter (*PFDM*) model. This model was first introduced in [50], [51] and then further works were done in [52]. Recently, *PFDM* model has been studied using cosmological constant in [54]-[56]. Also shadow of rotating black hole in *PFDM* has been worked out in [58]. Besides there is a review work on the analytical study of black hole shadow in [59].

We plan to study the shadow of charged rotating black hole in perfect fluid dark matter (*PFDM*) surrounded by plasma. In a general scenario black holes remain surrounded by material media. Hence we take interest to investigate the general case where black holes are surrounded by some medium. Study of black hole shadows considering plasma has been conducted in [60]-[69]. We aim to study black hole shadow considering radial power law distribution of plasma. Also we wish to consider cases of both homogenous [70] and inhomogenous plasma.

The paper is organised as follows. In section 1, we give a brief overview of the literature in studies of black hole shadow in general and in presence of plasma. In section 2, we discuss the system of rotating charged black hole in *PFDM*. Then in section 3, we continue the subsequent discussion of the black hole system in presence of plasma. Later in section 4, we discuss the circular geodesics. Here we focus in studying the co-rotating and counter rotating photon orbits moving in the equatorial plane. Then we study the black hole shadow in near equatorial plane. In section 5, we study the impact of the spacetime parameters (a , Q , χ , k) on the shadow of the black hole. Later in section 6 we look into the effective potential (V_{eff}) as encountered by the photons in the black hole spacetime. Finally in section 7, we conclude by discussing our observations in detail. We work in geometric units, where we consider $c = G = 1$. Apart from the discussion and analysis, all our mathematical calculations and results are obtained using $M = 1$.

2 Black hole spacetime in perfect fluid dark matter

We shall consider a charged black hole surrounded by perfect fluid dark matter (*PFDM*). The corresponding action in (3+1) dimensions is given as [1]

$$S = \int d^4x \sqrt{-g} \left(\frac{R}{16\pi G} + \frac{1}{4} F^{\mu\nu} F_{\mu\nu} + \mathcal{L}_{DM} \right) \quad (1)$$

with R being the Ricci scalar and $F_{\mu\nu}$ being the Maxwell field strength tensor. \mathcal{L}_{DM} gives the Lagrangian density of the *PFDM*. Extremizing the action gives the Einstein field equations

$$R_{\mu\nu} - \frac{1}{2} g_{\mu\nu} R = 8\pi G (T_{\mu\nu}^M - T_{\mu\nu}^{DM}) . \quad (2)$$

In the above equation, $T_{\mu\nu}^M$ and $T_{\mu\nu}^{DM}$ are the energy-momentum tensor of ordinary matter and *PFDM* respectively. The components of energy-momentum tensor in both cases can be expressed as [53], [54]

$$(T_{\nu}^{\mu})^M = \text{diag} \left(-\frac{Q^2}{8\pi G r^4}, -\frac{Q^2}{8\pi G r^4}, \frac{Q^2}{8\pi G r^4}, \frac{Q^2}{8\pi G r^4} \right) \quad (3)$$

$$(T_{\nu}^{\mu})^{DM} = \text{diag}(-\rho, P_r, P_\theta, P_\phi) = \text{diag}(-\rho, -\rho, P, P) \quad (4)$$

where Q is the black hole charge, ρ and P are the energy density and pressure of *PFDM* respectively. The solution of Einstein's field equations take the form [1]

$$ds^2 = -f(r) dt^2 + \frac{1}{f(r)} dr^2 + r^2 d\theta^2 + r^2 \sin^2 \theta d\phi^2 \quad (5)$$

with $f(r)$ being given by

$$f(r) = 1 - \frac{2GM}{r} + \frac{Q^2}{r^2} + \frac{\chi}{r} \ln \left(\frac{r}{|\chi|} \right) . \quad (6)$$

M gives the mass of the black hole and χ is an integration constant and corresponds to the *PFDM* parameter. The energy conditions on the energy-momentum tensor constraints χ to take only positive values. The rotating version of the solution is obtained using Newman-Janis algorithm in [1]. The solution has the form

$$ds^2 = -\frac{1}{\rho^2}(\Delta - a^2 \sin^2 \theta) dt^2 + \frac{\rho^2}{\Delta} dr^2 + \rho^2 d\theta^2 - \frac{2a \sin^2 \theta}{\rho^2} [r^2 + a^2 - \Delta] dt d\phi + \sin^2 \theta \left[r^2 + a^2 + \frac{a^2 \sin^2 \theta}{\rho^2} (r^2 + a^2 - \Delta) \right] d\phi^2 \quad (7)$$

with

$$\Delta = r^2 + a^2 - 2Mr + Q^2 + \chi r \ln \left(\frac{r}{|\chi|} \right), \quad \rho^2 = r^2 + a^2 \cos^2 \theta. \quad (8)$$

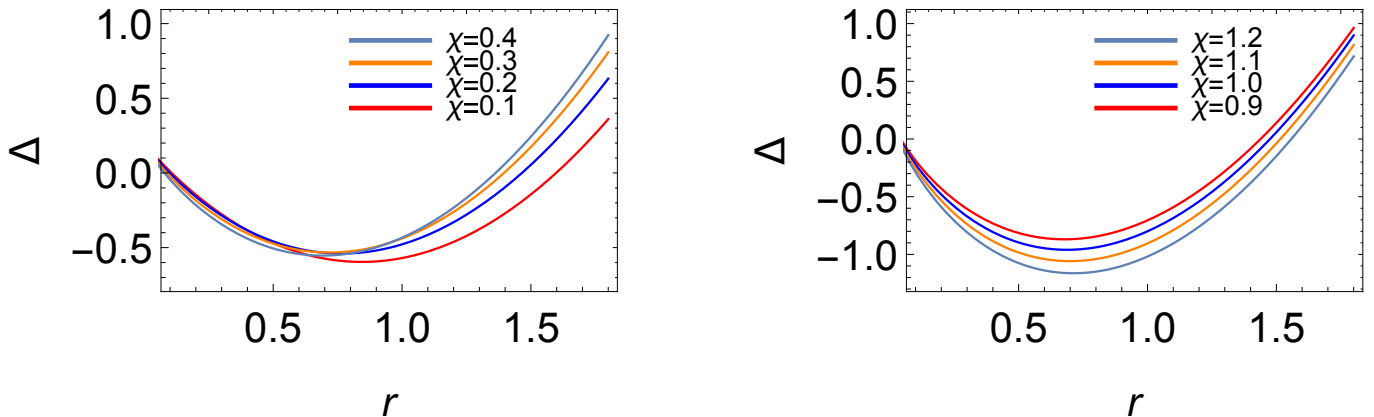


Figure 1: Plot for $\Delta(r)$ with respect to r for $a=0.4$, $Q=0.2$ for $\chi < \chi_c$ (left panel) and $\chi > \chi_c$ (right panel) with $\chi_c = 0.498$.

On analysing the spacetime, we find that the black hole has two horizons. The presence of *PFDM* does not increase the number of horizons of the black hole. Yet it does modify the location of the horizon surface which can be observed by analysing Δ . The black hole event horizon can be obtained by using the condition $\Delta = 0$.

a	Q	χ_c
0.1	0.2	0.529
0.3	0.2	0.513
0.5	0.2	0.477

a	Q	χ_c
0.4	0.0	0.508
0.4	0.3	0.488
0.4	0.6	0.414

Table 1: Table showing the variation of the critical value of *PFDM* parameter χ_c with black hole spin a and charge Q .

Using this condition, we find that χ is a function of M , a and Q . Besides, we also observe that for fixed values of M , a and Q , as we increase the *PFDM* parameter χ , the outer event horizon (r_{h+}) initially decreases upto a critical value (χ_c) and then starts increasing. The inner event horizon (r_{h-}) decreases all through. The reason for such an observation can be assigned to the fact that *PFDM* contributes to the mass of the system [58]. We can explain this observation by asserting that the system is a composition of two parts, original black hole of mass M and the black hole corresponding to *PFDM* with mass M_0 . When $\chi < \chi_c$, then the total system mass is given by M with an inhibition from *PFDM* mass M_0 . As χ increases, the inhibition increases which gets reflected in the black hole event horizon (r_{h+}). Just at the point when

$\chi \geq \chi_c$, *PFDM* mass M_0 becomes greater than original black hole mass M and hence the effective mass and the effective horizon is depicted by the mass of the *PFDM*. Thus with increase in χ , event horizon radius (r_{h+}) starts increasing.

3 Rotating charged black hole with perfect fluid dark matter immersed in plasma

Here we consider the rotating charged black hole surrounded by *PFDM* immersed in plasma. We assume that there is no interaction between *PFDM* and plasma. The consideration of plasma is realistic, since most black holes are surrounded by material media. Plasma is a dispersive medium where light rays deviate depending on their frequency. The Hamiltonian for the light rays can be derived using Maxwell's equations considering the source to be made of two charged fluids (electrons and ions). For the study of plasma in curved background, we can consider magnetised [71] as well as non-magnetised plasma [72]. In our study we consider non-magnetised, pressureless (dustlike) plasma. The Hamiltonian for light rays in presence of plasma in curved spacetime is provided in [73]. It is applicable even in our case, since dark matter doesn't interact with plasma by other means except gravity. The Hamiltonian has the form [60]

$$H(x^\mu, p_\mu) = \frac{1}{2} \left[g^{\mu\nu} p_\mu p_\nu + \omega_p(r)^2 \right] \quad (9)$$

where $\omega_p(r)$ is the plasma frequency considered to have radial dependence only. The refractive index (n) of the material medium depends on both the plasma frequency (ω_p) as well the frequency of photons (ω) measured by a static observer. The expression of $n(r, \omega)$ has the form [74]

$$n^2(r, \omega) = 1 - \left(\frac{\omega_p(r)}{\omega} \right)^2. \quad (10)$$

For an observer having 4-velocity u^μ , the effective energy of photon as measured by the observer is $\hbar\omega = -p_\mu u^\mu$. In our case, the observer is static, hence $\hbar\omega = -p_0 u^0 = -p_0 \sqrt{-g^{00}}$ [74]. Replacing the expressions for the refractive index of plasma medium and photon energy in eq.(9), the Hamiltonian becomes

$$H(x^\mu, p_\mu) = \frac{1}{2} \left[g^{\mu\nu} p_\mu p_\nu - (n^2 - 1) \left(p_0 \sqrt{-g^{00}} \right)^2 \right]. \quad (11)$$

In order to solve for the geodesics, we need to have an explicit form for the plasma frequency ω_p . Since ω_p depends only on r , plasma can have many forms of distribution. Here we assume an extensively studied distribution in the literature, the radial power law distribution, with ω_p given as

$$\omega_p^2 = \frac{4\pi e^2 N(r)}{m_e} \quad (12)$$

where e is the electronic charge, m_e is the mass of the electron and $N(r)$ being the plasma number density. The plasma density following [73], [74] has the form

$$N(r) = \frac{N_0}{r^h}. \quad (13)$$

where N_0 is a constant, h can take integer values with $h \geq 0$. The final form of the refractive index $n(r)$ along with $\frac{\omega_p}{\omega}$ becomes

$$\left(\frac{\omega_p}{\omega} \right)^2 = \frac{k}{r^h}; \quad n(r) = \sqrt{1 - \frac{k}{r^h}}. \quad (14)$$

Here k is a constant which gives the weightage of plasma around the black hole, also $h = 1, 2, 3$ [74]. In this study we shall consider $h = 0$ which results in $n(r) = \text{constant}$ corresponding to homogenous plasma media. Later we will consider the simplest dependence on r with $h = 1$. The second case will be regarded as inhomogenous plasma distribution.

4 Study of circular geodesics in plasma medium

4.1 Co-rotating and counter rotating photon orbits

The photons in the rotating black hole spacetime can move along the direction of black hole spin (co-rotating photons) as well as opposite to that of black hole spin (counter rotating photons). In order to determine the radius (r_p) of those photon orbits, we need to determine the radial geodesic equation and impose the condition for circular geodesics. For this, we need to use the Hamiltonian (\mathcal{H}) to determine the trajectories of the particles in the equatorial plane. The Hamiltonian given in eq.(11) takes the form

$$\mathcal{H} = \frac{1}{2} \left[g^{\mu\nu} p_\mu p_\nu + (n^2 - 1) g^{00} p_0^2 \right] \quad (15)$$

with $\mathcal{H} = 0$ for photons. Since we are interested in the geodesics of the equatorial plane, we set $\theta = \frac{\pi}{2}$ and thus $\dot{\theta} = 0$. The geodesics can be calculated using Hamilton's equation of motion given by

$$\dot{x}^\mu = \frac{\partial \mathcal{H}}{\partial p_\mu} \quad ; \quad \dot{p}_\mu = -\frac{\partial \mathcal{H}}{\partial x^\mu} . \quad (16)$$

The Hamiltonian depends on the metric ($g_{\mu\nu}$) as well as on the refractive index of plasma ($n(r)$). The metric has no explicit dependence on $x_0 (= t)$ and $x_3 (= \phi)$. So the Hamilton's second equation of motion gives two constants of motion $p_0 = -E$ and $p_3 = L_\phi$. E and L_ϕ respectively give the energy per unit mass and angular momentum per unit mass of the photon as observed by a stationary observer at infinity. The geodesics corresponding to t and ϕ in the equatorial plane becomes

$$r^2 \dot{t} = \frac{r^2 + a^2}{\Delta} \left[n^2 (r^2 + a^2) E - a L_\phi \right] + a \left[L_\phi - a n^2 E \right] \quad (17)$$

$$r^2 \dot{\phi} = \frac{a}{\Delta} \left[(r^2 + a^2) E - a L_\phi \right] + \left[L_\phi - a E \right] . \quad (18)$$

Now $p_r = \frac{\partial \mathcal{L}}{\partial \dot{r}} = \frac{\partial \mathcal{S}}{\partial r} = g_{rr} \dot{r}$ with $\mathcal{L} = \frac{1}{2} g_{\mu\nu} \dot{x}^\mu \dot{x}^\nu$. The dot in the above equations correspond to derivative with respect to the affine parameter λ . Since light rays cannot be parametrized in terms of proper time (τ), so we need to parametrize them with some other parameter. This parametrization is done using the affine parameter (λ). With the above equations in hand, we get from eq.(15)

$$\dot{r}^2 = \frac{1}{r^4} \left[\left(E(r^2 + a^2) - a L_\phi \right)^2 - \Delta (a E - L_\phi)^2 + (n^2 - 1) \left(E^2 (r^2 + a^2)^2 - \Delta E^2 a^2 \right) \right] . \quad (19)$$

In order to obtain the two kinds of orbits discussed above, we define the impact parameter as $\frac{L_\phi}{E} = D$, in terms of which the radial eq.(19) looks as

$$\dot{r}^2 = \frac{E^2}{r^4} \left[\left((r^2 + a^2) - a D \right)^2 - \Delta (a - D)^2 + (n^2 - 1) \left((r^2 + a^2)^2 - \Delta a^2 \right) \right] . \quad (20)$$

Rearranging eq.(20), we have

$$\frac{r^2 \dot{r}^2}{E^2} = \frac{1}{r^2} \left[\left((r^2 + a^2) - a D \right)^2 - \Delta (a - D)^2 + (n^2 - 1) \left((r^2 + a^2)^2 - \Delta a^2 \right) \right] = F(r) . \quad (21)$$

Imposing the condition for circular geodesics, that is, $F(r) = 0 = F'(r)$, we get

$$r^2 + (a^2 - D^2) + \frac{2M}{r} (a - D)^2 - \frac{Q^2}{r^2} (a - D)^2 - \frac{\chi}{r} (a - D)^2 \ln \left(\frac{r}{|\chi|} \right) + (n^2 - 1) \left(r^2 + a^2 + a^2 \left(\frac{2M}{r} - \frac{Q^2}{r^2} - \frac{\chi}{r} \ln \left(\frac{r}{|\chi|} \right) \right) \right) = 0 . \quad (22)$$

$$2r - \frac{2M}{r^2}(a-D)^2 + \frac{2Q^2}{r^3}(a-D)^2 + \frac{\chi}{r^2}(a-D)^2 \ln\left(\frac{r}{|\chi|}\right) - \frac{\chi}{r^2}(a-D)^2 + (n^2-1)\left(2r - a^2\left(\frac{2M}{r^2} - \frac{2Q^2}{r^3} - \frac{\chi}{r^2} \ln\left(\frac{r}{|\chi|}\right) + \frac{\chi}{r^2}\right)\right) + 2nn'\left(r^2 + a^2 + a^2\left(\frac{2M}{r} - \frac{Q^2}{r^2} - \frac{\chi}{r} \ln\left(\frac{r}{|\chi|}\right)\right)\right) = 0 \quad (23)$$

where, $n' \equiv \frac{dn}{dr}$. Solving for $(a-D)$ in eq.(23), we have

$$(a-D) = \pm \sqrt{\frac{2r^5 + (n^2-1)\left[2r^5 - a^2\left(2Mr^2 - 2Q^2r - \chi r^2 \ln\left(\frac{r}{|\chi|}\right) + \alpha r^2\right)\right] + 2nn'\left[r^4(r^2 + a^2) + a^2\left(2Mr^3 - Q^2r^2 - \chi r^3 \ln\left(\frac{r}{|\chi|}\right)\right)\right]}{2Mr^2 - 2Q^2r - \chi r^2 \ln\left(\frac{r}{|\chi|}\right) + \chi r^2}}}. \quad (24)$$

Thus the impact parameter becomes

$$D = a \mp \sqrt{\frac{2r^5 + (n^2-1)\left[2r^5 - a^2\left(2Mr^2 - 2Q^2r - \chi r^2 \ln\left(\frac{r}{|\chi|}\right) + \chi r^2\right)\right] + 2nn'\left[r^4(r^2 + a^2) + a^2\left(2Mr^3 - Q^2r^2 - \chi r^3 \ln\left(\frac{r}{|\chi|}\right)\right)\right]}{2Mr^2 - 2Q^2r - \chi r^2 \ln\left(\frac{r}{|\chi|}\right) + \chi r^2}}}. \quad (25)$$

The \mp sign corresponds to counter and co-rotating geodesics of photons moving in the black hole spacetime. In case of background devoid of plasma, that is, $n = 1, n' = 0$ we have

$$D = a \mp \sqrt{\frac{2r^5}{2Mr^2 - 2Q^2r - \chi r^2 \ln\left(\frac{r}{|\chi|}\right) + \chi r^2}} \quad (26)$$

which corresponds to the expression derived in [1]. Replacing D from eq.(25) in eq.(22) we get an equation in r devoid of the constants E and L_ϕ which depends only on the spacetime parameters (M, Q, χ, n) . The solution of the equation gives the photon orbit radius (r_p) both for co-rotating and counter rotating orbits. The table(s) below show the photon orbit radius (r_p) both for co and counter rotating orbits with variation in plasma parameter (k).

$\chi = 0.2$		$\chi = 1.0$		$\chi = 0.2$		$\chi = 1.0$	
k	r_{p1}	k	r_{p1}	k	r_{p1}	k	r_{p1}
0.0	1.645	0.0	1.742	0.0	1.645	0.0	1.742
0.2	1.480	0.2	1.632	0.2	1.507	0.2	1.632
0.27	1.381	0.38	1.418	0.31	1.385	0.4	1.492

Table 2: Radius (r_{p1}) for co-rotating (prograde) photon orbits with variation in plasma parameter (k) with black hole spin $a=0.5$ and charge $Q=0.3$. The first two are for homogenous plasma ($n = \sqrt{1-k}$) and the next two for inhomogenous plasma ($n = \sqrt{1-\frac{k}{r}}$).

Table 2 show that with increase in the plasma parameter k , the radius of co-rotating photon orbits r_{p1} decrease in case of both homogenous and inhomogenous plasma. Besides they exist closer to the event horizon (r_{h+}) of the black hole. The effect of plasma parameter k on the radius of the orbits remains same for both $\chi < \chi_c$ and $\chi > \chi_c$. The critical value (χ_c) of the *PFDM* parameter χ for black hole spin $a = 0.5$ and charge $Q = 0.3$ is 0.467. Also we find that the photon orbits do not exist for all possible values of the plasma parameter k . After a certain critical value of plasma parameter $k = k_c$, the photon radius drops below the event horizon radius (r_{h+}) and thus has no physical existence. Thus there is a bound to the value of k depending on the combinations of the black hole parameters (M, Q, χ) .

Table 3 show that with increase in plasma parameter k , the radius of counter rotating photon orbits r_{p2} increase in case of homogenous plasma distribution whereas it decreases in case of inhomogenous distribution. The effect of plasma parameter k on the radius of the orbits remains same for both $\chi < \chi_c$ and $\chi > \chi_c$. Here too only for a certain combination of spacetime parameters and plasma parameter k does the photon orbits exist which results in a bound on the plasma parameter k .

4.2 Black hole shadow

In this section, we wish to calculate the black hole shadow. Shadows are formed due to bending of light rays near regions of strong gravity. In case of black holes, when light from a distant source comes near to

$\chi = 0.2$	
k	r_{p2}
0.0	2.782
0.2	2.825
0.4	2.886

$\chi = 1.0$	
k	r_{p2}
0.0	2.608
0.2	2.640
0.4	2.685

$\chi = 0.2$	
k	r_{p2}
0.0	2.782
0.2	2.761
0.4	2.737

$\chi = 1.0$	
k	r_{p2}
0.0	2.608
0.2	2.587
0.4	2.564

Table 3: Radius (r_{p2}) for counter rotating (retrograde) photon orbits with variation in plasma parameter (k) with black hole spin $a=0.5$ and charge $Q=0.3$. The first two are for homogenous plasma ($n = \sqrt{1-k}$) and the next two for inhomogenous plasma ($n = \sqrt{1 - \frac{k}{r}}$).

it, light rays get deflected. The deflected rays after encircling the black hole either plunges into the black hole or escapes to infinity. These light rays orbit in unstable circular orbits. Light rays from the unstable orbits reaches the observer at infinity and creates *circular* or *deformed circular* boundary curve. The dark disk inside the curve is called the black hole shadow. Thus in order to determine the shadow, we need to the geodesics of light rays (photons) which have been determined already in the earlier section for t and ϕ for $\theta = \frac{\pi}{2}$. The expressions for \dot{t} and $\dot{\phi}$ in arbitrary plane reads

$$\rho^2 \dot{t} = \frac{r^2 + a^2}{\Delta} \left[n^2 (r^2 + a^2) E - a L_\phi \right] + a \left[L_\phi - a n^2 E \sin^2 \theta \right] \quad (27)$$

$$\rho^2 \dot{\phi} = \frac{a}{\Delta} \left[(r^2 + a^2) E - a L_\phi \right] + \left[L_\phi \csc^2 \theta - a E \right]. \quad (28)$$

In order to evaluate the geodesics for r and θ , we use the Hamilton-Jacobi equation, which reads

$$\frac{\partial S}{\partial \lambda} = -\mathcal{H} = -\frac{1}{2} \left[g^{\mu\nu} \left(\frac{\partial S}{\partial x^\mu} \right) \left(\frac{\partial S}{\partial x^\nu} \right) + (n^2 - 1) g^{00} \left(\frac{\partial S}{\partial x^0} \right)^2 \right]. \quad (29)$$

In order to solve the above equation, we need to choose an ansatz for S . Following [75], we use

$$S = -Et + L_\phi \phi + S_r(r) + S_\theta(\theta). \quad (30)$$

Replacing S in eq.(29), we have

$$\begin{aligned} & -\frac{(n^2 - 1)}{\Delta} E^2 (r^2 + a^2)^2 - \frac{1}{\Delta} \left[(r^2 + a^2) E - a L_\phi \right]^2 + n^2 a^2 E^2 \sin^2 \theta - a^2 E^2 \\ & + L_\phi^2 \cot^2 \theta + (aE - L_\phi)^2 + \Delta \left(\frac{\partial S_r}{\partial r} \right)^2 + \left(\frac{\partial S_\theta}{\partial \theta} \right)^2 = 0. \end{aligned} \quad (31)$$

Now we wish to separate the above equation in r and θ variables. By inspecting the term $n(r)^2 a^2 E^2 \sin^2 \theta$, we find that it is in general, not possible to separate $n(r)$ from $\sin \theta$. We need to take special cases, I. Set $\theta = \frac{\pi}{2}$, that is consider the motion of light rays in the equatorial plane, II. Choose $n(r) = \text{constant}$, which is possible only for homogenous plasma distribution. We shall consider case I here.

Choosing a near equatorial plane and setting $\theta = \frac{\pi}{2} + \epsilon$, ($\epsilon \ll 1$), we have eq.(31) as

$$\begin{aligned} & -\frac{(n^2 - 1)}{\Delta} E^2 (r^2 + a^2)^2 - \frac{1}{\Delta} \left[(r^2 + a^2) E - a L_\phi \right]^2 + (n^2 - 1) a^2 E^2 \\ & + (aE - L_\phi)^2 + \Delta \left(\frac{\partial S_r}{\partial r} \right)^2 + \left(\frac{\partial S_\epsilon}{\partial \epsilon} \right)^2 = 0. \end{aligned} \quad (32)$$

Introducing a constant of separation κ , known as Carter constant [75], we can split the equation into two parts as

$$\begin{aligned} & \frac{(n^2 - 1)}{\Delta} E^2 (r^2 + a^2)^2 + \frac{1}{\Delta} \left[(r^2 + a^2) E - a L_\phi \right]^2 - (n^2 - 1) a^2 E^2 \\ & - (aE - L_\phi)^2 - \Delta \left(\frac{\partial S_r}{\partial r} \right)^2 = \left(\frac{\partial S_\epsilon}{\partial \epsilon} \right)^2 = \kappa. \end{aligned} \quad (33)$$

Finally, using $\frac{\partial \mathcal{L}}{\partial \dot{x}^\mu} = \frac{\partial S}{\partial x^\mu}$, where $\mathcal{L} = \frac{1}{2}g_{\mu\nu}\dot{x}^\mu\dot{x}^\nu$, we get equation(s) for r and ϵ as

$$r^2\dot{r} = \sqrt{R(r)} \quad (34)$$

$$r^2\dot{\epsilon} = \sqrt{\Theta(\epsilon)} \quad (35)$$

where the expressions for $R(r)$ and $\Theta(\epsilon)$ takes the form

$$R(r) = (n^2 - 1)E^2(r^2 + a^2)^2 + \left[(r^2 + a^2)E - aL_\phi\right]^2 - \Delta \left[(n^2 - 1)a^2E^2 + (aE - L_\phi)^2 + \kappa\right] \quad (36)$$

$$\Theta(\epsilon) = \kappa. \quad (37)$$

Since, shadows are formed by light rays moving in unstable circular orbits, so we use the conditions $R(r) = \frac{\partial R(r)}{\partial r} = 0$. We define $\xi = \frac{L_\phi}{E}$ and $\eta = \frac{\kappa}{E^2}$, which are known as Chandrasekhar constants [75]. The conditions for unstable circular orbits constrain ξ and η . The conditions read

$$(n^2 - 1)(r^2 + a^2)^2 + \left[(r^2 + a^2) - a\xi\right]^2 = \Delta \left[(n^2 - 1)a^2 + (a - \xi)^2 + \eta\right] \quad (38)$$

$$4r(n^2 - 1)(r^2 + a^2) + 4r\left[(r^2 + a^2) - a\xi\right] - 2nn'\Delta a^2 + 2(r^2 + a^2)nn' = \Delta' \left[(n^2 - 1)a^2 + (a - \xi)^2 + \eta\right]. \quad (39)$$

Eliminating η from the above equations, we get a quadratic equation ξ as

$$A\xi^2 + 2B\xi + C = 0 \quad (40)$$

with the expressions for A , B and C taking the form

$$\begin{aligned} A &= a^2\Delta' ; \quad B = 2ar\Delta - a\Delta'(r^2 + a^2) ; \\ C &= \left[n^2\Delta'(r^2 + a^2)^2 - 4r\Delta n^2(r^2 + a^2) + 2nn'\Delta^2 a^2 - 2(r^2 + a^2)^2 nn'\Delta\right]. \end{aligned} \quad (41)$$

Solving for ξ , we have

$$\xi = -\frac{B}{A} \pm \sqrt{\left(\frac{B}{A}\right)^2 - \frac{C}{A}} \quad (42)$$

with the negative sign yielding the appropriate results. The expression for η becomes

$$\eta = \frac{1}{\Delta} \left[(n^2 - 1)(r^2 + a^2)^2 + \left[(r^2 + a^2) - a\xi\right]^2 \right] - (n^2 - 1)a^2 - (a - \xi)^2. \quad (43)$$

The constants ξ and η are the quantities in terms of which shadow radius R_s is evaluated.

As mentioned earlier, black hole shadow is a dark planar disk encircled by light rays. Since the shadow is formed in a plane, it is characterised by two coordinates, namely, the celestial coordinates designated by α and β . These coordinates are applicable for observers at infinity. They take the form

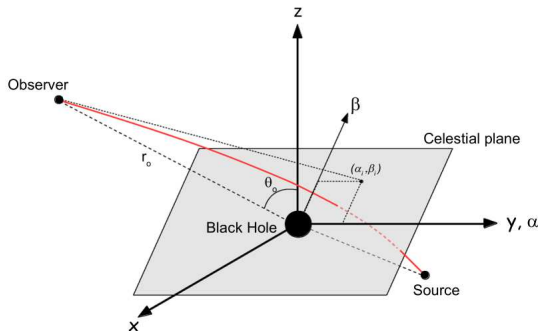


Figure 2: Celestial coordinates (α, β) [28].

$$\alpha = \lim_{r_0 \rightarrow \infty} -r_0^2 \sin \theta_0 \left(\frac{d\phi}{dr} \right) = \lim_{r_0 \rightarrow \infty} -r_0^2 \left(\frac{d\phi}{dr} \right) \quad (44)$$

$$\beta = \lim_{r_0 \rightarrow \infty} r_0^2 \left(\frac{d\epsilon}{dr} \right). \quad (45)$$

As can be seen from Fig.2, we consider a black hole residing between the source and the observer. We have shown a tangent on the light ray at the point where light reaches the observer. The light ray meets the celestial plane at the point (α, β) . Considering all light rays from all possible directions and drawing tangents that intersect the plane, we get a circular or near circular or deformed circular boundary curve. The coordinate α gives the apparent perpendicular distance of the shadow boundary from the axis of black hole rotation and the coordinate β gives the apparent perpendicular distance of the boundary of the shadow from its projection in the equatorial plane. r_0 gives the radial distance of the observer from the black hole and θ_0 corresponds to the inclination angle of the observer's line of sight with the axis of rotation. In our case, we consider the observer to be in the equatorial plane, that is, $\theta_0 = \frac{\pi}{2}$.

In order to determine α and β , we need the geodesic equations and thereby calculate $\left(\frac{d\phi}{d\lambda}\right)$ and $\left(\frac{d\epsilon}{dr}\right)$. The geodesics for ϕ , ϵ and r have the form (considering near equatorial plane)

$$\left(\frac{d\phi}{d\lambda}\right) = \frac{a}{\Delta r^2} \left[(r^2 + a^2)E - aL_\phi \right] + \frac{1}{r^2} \left[L_\phi - aE \right] \quad (46)$$

$$\left(\frac{d\epsilon}{d\lambda}\right) = \frac{\sqrt{\kappa}}{r^2} \quad (47)$$

$$\left(\frac{dr}{d\lambda}\right) = \frac{1}{r^2} \sqrt{(n^2 - 1)E^2(r^2 + a^2)^2 + \left[(r^2 + a^2)E - aL_\phi \right]^2 - \Delta \left[(n^2 - 1)a^2E^2 + (aE - L_\phi)^2 + \kappa \right]}. \quad (48)$$

Utilising the above geodesics, we get the relevant equations as

$$\left(\frac{d\phi}{dr}\right) = \frac{\frac{a}{\Delta} \left[(r^2 + a^2)E - aL_\phi \right] + \left[L_\phi \csc^2 \theta - aE \right]}{\sqrt{(n^2 - 1)E^2(r^2 + a^2)^2 + \left[(r^2 + a^2)E - aL_\phi \right]^2 - \Delta \left[(n^2 - 1)a^2E^2 + (aE - L_\phi)^2 + \kappa \right]}} \quad (49)$$

$$\left(\frac{d\epsilon}{dr}\right) = \frac{\kappa}{\sqrt{(n^2 - 1)E^2(r^2 + a^2)^2 + \left[(r^2 + a^2)E - aL_\phi \right]^2 - \Delta \left[(n^2 - 1)a^2E^2 + (aE - L_\phi)^2 + \kappa \right]}}. \quad (50)$$

Now replacing the above relations in the expressions for α and β and then taking the limit $r \rightarrow \infty$, we get the celestial coordinates as

$$\alpha = -\frac{\xi}{n} \quad ; \quad \beta = \pm \frac{\sqrt{\eta}}{n}. \quad (51)$$

This relation is valid for both homogenous and inhomogenous plasma distribution. Plotting α along X-axis vs β along Y-axis, we get the silhouette of the black hole shadow.

5 Impact of the spacetime, *PFDM* and plasma parameters on the black hole shadow

The motion of any particle in the black hole spacetime is influenced by the parameters describing the spacetime. The same is true for unstable photons ($m = 0$) that either plunge into the black hole singularity or fly off to infinity. Those that fly off to infinity reach the observer and form the boundary of the black hole shadow. Thus the shadow formed by photons gets impacted by the spacetime parameters.

The parameters describing the spacetime are spin (a) and charge (Q) of the black hole, *PFDM* parameter (χ) and the plasma parameter (k). Now we show the plots and discuss how the parameters affect the black hole shadow.

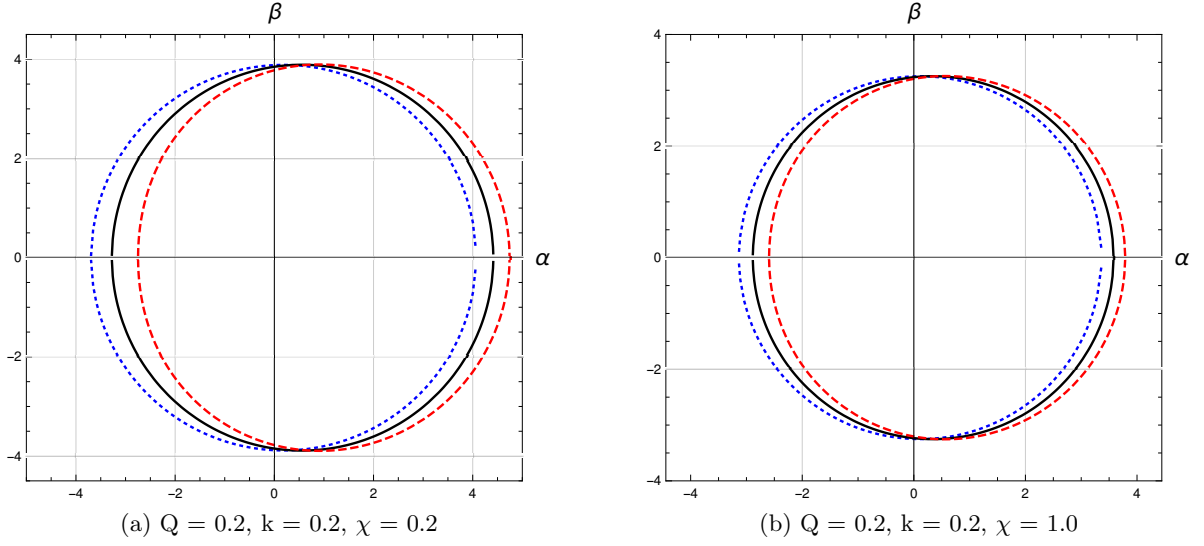


Figure 3: Variation of the black hole shadow with spin (a) of the black hole. The colored plots are for different spin values-blue dotted ($a = 0.1$), black ($a = 0.3$), red dashed ($a = 0.5$).

In the Fig.3, we have shown the impact of the black hole spin (a) on the shadow. In order to do so, we have fixed the rest of the black hole parameters ($Q = 0.2$, $\chi = 0.2, 1.0$, $k = 0.2$). Previously, we have mentioned that $PFDM$ parameter χ has two ranges of values separated by χ_c . The left plot is for $\chi < \chi_c$ and the right one is for $\chi > \chi_c$. The value of χ_c varies with variation in the values of black hole spin a with fixed charge Q as can be seen in Table 1. The shadow is larger in case of $\chi < \chi_c$, whereas, they are comparatively smaller in case of $\chi > \chi_c$. Besides, we find that with the increase in spin (a) of the black hole, the shadow gets rotated and slightly deformed. This is due to the rotational drag force on the unstable photons moving in close vicinity of the black hole.

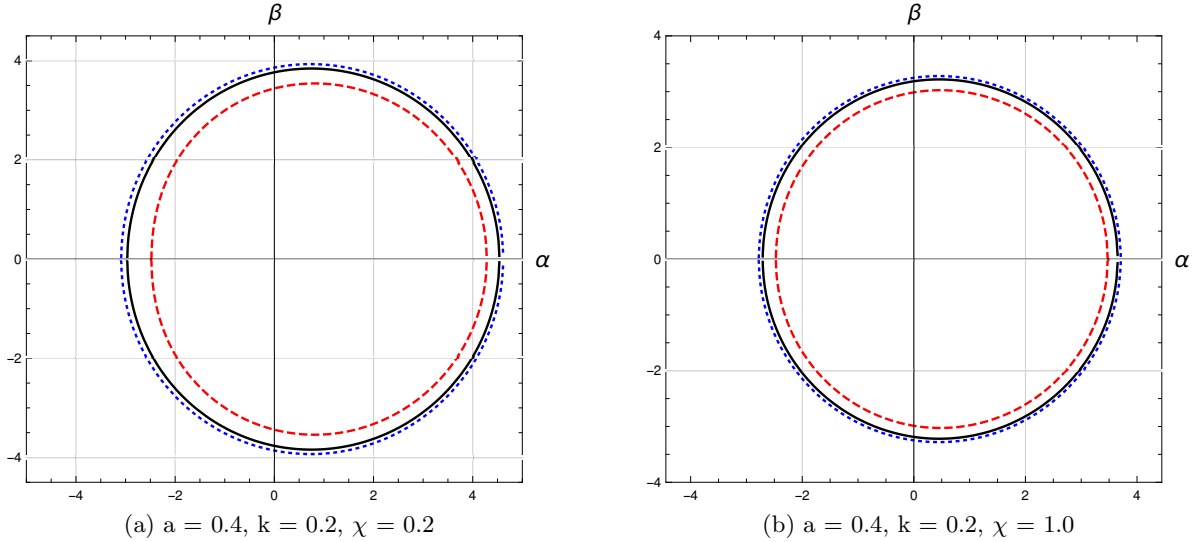


Figure 4: Variation of the black hole shadow with charge Q . The colored plots are for different charge values-blue dotted ($Q = 0.0$), black ($Q = 0.3$), red dashed ($Q = 0.6$).

Fig.4 depict the effect of charge (Q) on the shadow of the black hole. Just like the previous case we have shown two ranges of χ ($\chi < \chi_c$ and $\chi > \chi_c$). We set the rest of the black hole parameters to constant values ($a = 0.4$, $\chi = 0.2, 1.0$, $k = 0.2$). In this case too, the value of χ_c varies with variation in the values of black hole charge Q with fixed spin a as can be seen in Table 1. Here too, we find that the shadow size in $\chi < \chi_c$ is greater than that in $\chi > \chi_c$. Also with the increase in charge (Q) of the black hole, the shadow size reduces in both cases ($\chi < \chi_c$ and $\chi > \chi_c$). The reason for the observation can be assigned to the fact that the event horizon radius ($r_{h+} = M + \sqrt{M^2 - Q^2}$) without dark matter ($\chi=0$) and plasma ($k=0$) decreases

with increase in charge Q . The same persists in presence of χ and k . The black hole shadow which is a manifestation of the event horizon, thereby decreases. The decrement in shadow size with charge (Q) is non-uniform.

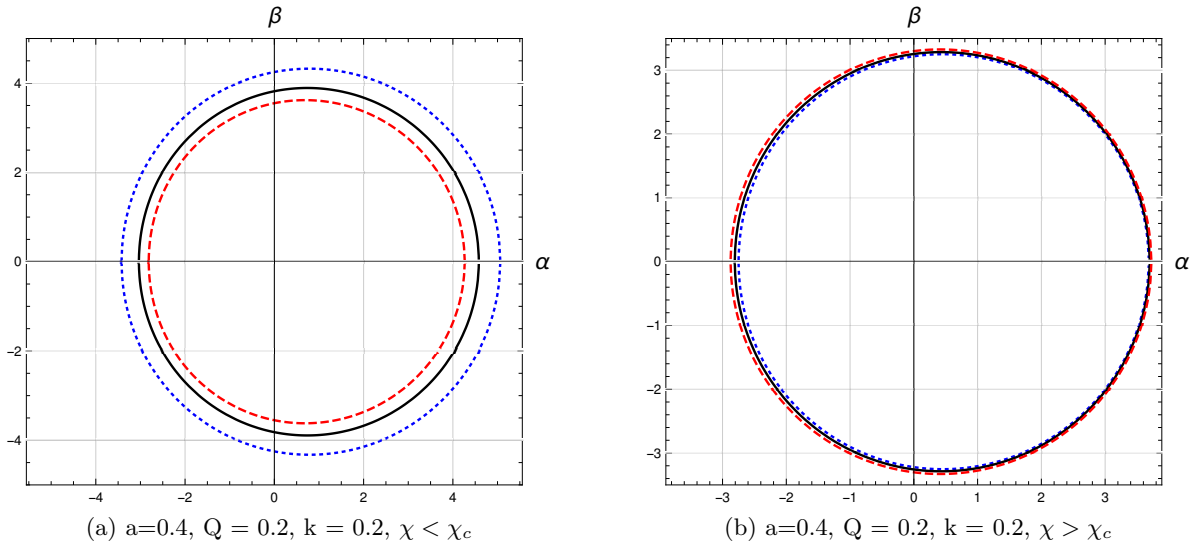


Figure 5: Variation of black hole shadow with perfect fluid dark matter ($PFDM$) parameter χ . The colored plots are for different values of χ -blue dotted ($\chi = 0.1$), black ($\chi = 0.2$), red dashed ($\chi = 0.3$) for the left plot and blue dotted ($\chi = 1.0$), black ($\chi = 1.1$), red dashed ($\chi = 1.2$) for the right plot.

In Fig.5, we have shown the impact of $PFDM$ parameter (χ) on the black hole shadow. From previous analysis, we find that the outer event horizon radius (r_{h+}) decreases with increase in χ for $\chi < \chi_c$ and increases for $\chi > \chi_c$. The analogical results are observed in case of black hole shadow. We found that for $\chi < \chi_c$, the shadow decreases non-uniformly and gets distorted with increase in χ . On the other hand, for $\chi > \chi_c$, the shadow increases uniformly with increase in χ , though the effect is less pronounced than for $\chi < \chi_c$. Such kind of observation results from the fact that $PFDM$ effectively gives the mass of the total system as discussed previously.

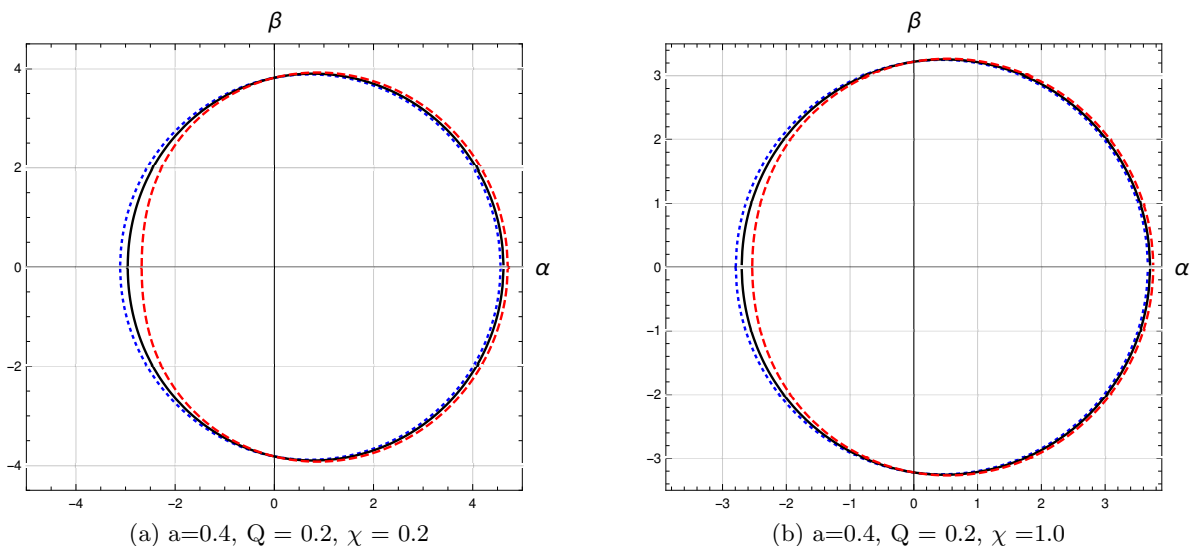


Figure 6: Variation of the black hole shadow with homogenous plasma ($n = \sqrt{1-k} = \text{constant}$). The colored plots are for different values of plasma parameter-blue dotted ($k = 0.0$), black ($k = 0.2$), red dashed ($k = 0.4$).

The effect of plasma is being observed for both homogenous and inhomogenous plasma distribution. In Fig.6 we have shown the effect of homogenous plasma ($n=\text{constant}$) on the black hole shadow. The observation is carried out in near equatorial plane. The extreme right point on the α axis corresponds to the radius of

counter rotating photon orbits [76]. On the other hand, the extreme left point on the α axis corresponds to the radius of co-rotating orbit. As seen earlier, the radius (r_{p1}) of co-rotating photons decrease with increase in plasma parameter k , whereas that of counter rotating photons (r_{p2}) increase with increase in k . The combination of the two orbits produces the shadow of the black hole. The same is observed both for $PFDM$ parameter $\chi = 0.2$ and 1.0 . Also the shadow size is larger in case of $\chi = 0.2$ with respect to that in $\chi = 1.0$.

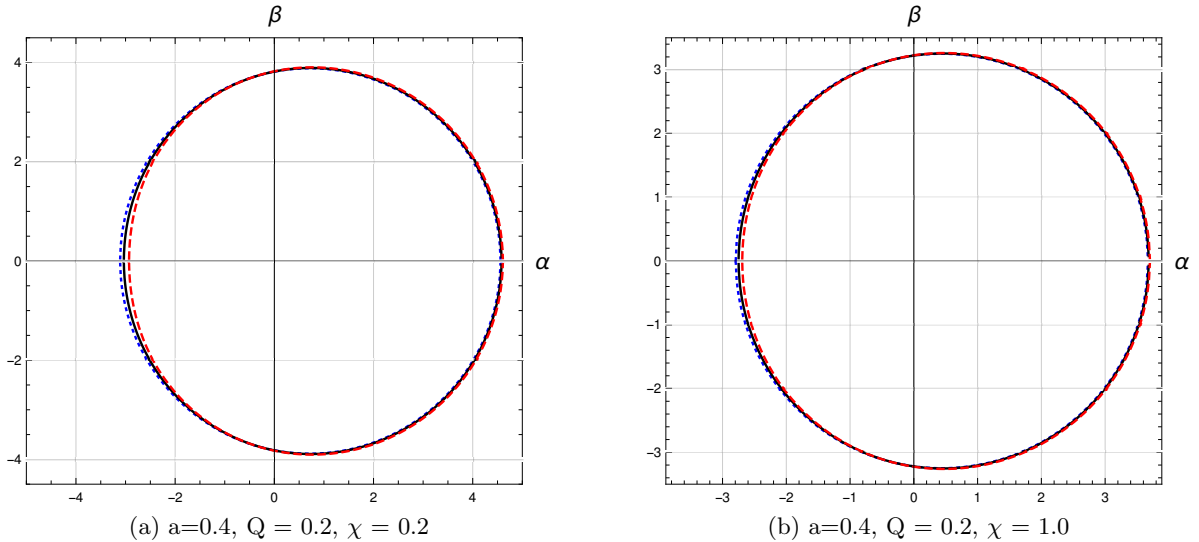


Figure 7: Variation of the black hole shadow with inhomogenous plasma ($n = n(r)$). The colored plots are for different values of plasma parameter-blue dotted ($k = 0.0$), black ($k = 0.2$), red dashed ($k = 0.4$).

We plot the effect of inhomogenous plasma ($n = n(r)$) on the black hole shadow in Fig.7. We show the plots both for $\chi < \chi_c$ and $\chi > \chi_c$. We observe that the co-rotating photon radius (r_{p1}) which correspond to the extreme left of α axis decreases with increase in plasma parameter k . The same happens in case of counter rotating radius (r_{p2}) which corresponds to the extreme right of the α axis. The effect is the same as obtained previously following a numerical approach. The cumulative effect of the two extreme orbit produces the unstable photon orbit which forms the black hole shadow. The effect remains identical for both $\chi < \chi_c$ and $\chi > \chi_c$. The shadow size is larger in case of $\chi < \chi_c$ than that in $\chi > \chi_c$.

6 Effective potential (V_{eff})

In this section, we study the effective potential (V_{eff}) as faced by a photon moving in the black hole spacetime. The potential can have maxima or minima which corresponds to the existence of unstable or stable orbits. The condition for maxima or minima are given as $\frac{\partial^2 V_{eff}}{\partial r^2} < 0$ and $\frac{\partial^2 V_{eff}}{\partial r^2} > 0$ respectively. The effective potential can be obtained from the modified radial equation which gives

$$\dot{r}^2 + V_{eff} = E^2 \quad (52)$$

with the effective potential given by

$$V_{eff} = -\frac{(a^2 E^2 - L_\phi^2)}{r^2} - \frac{2M}{r^3}(aE - L_\phi)^2 + \frac{Q^2}{r^4}(aE - L_\phi)^2 + \frac{\chi}{r^3}(aE - L_\phi)^2 \quad (53)$$

$$-(n^2 - 1) \left[E^2 + \frac{a^2 E^2}{r^2} + a^2 E^2 \left(\frac{2M}{r^3} - \frac{Q^2}{r^4} - \frac{\chi}{r^3} \ln \frac{r}{|\chi|} \right) \right]. \quad (54)$$

The plots for the effective potential are shown below. Here we basically focus on the dependence of the effective potential on the plasma parameter k .

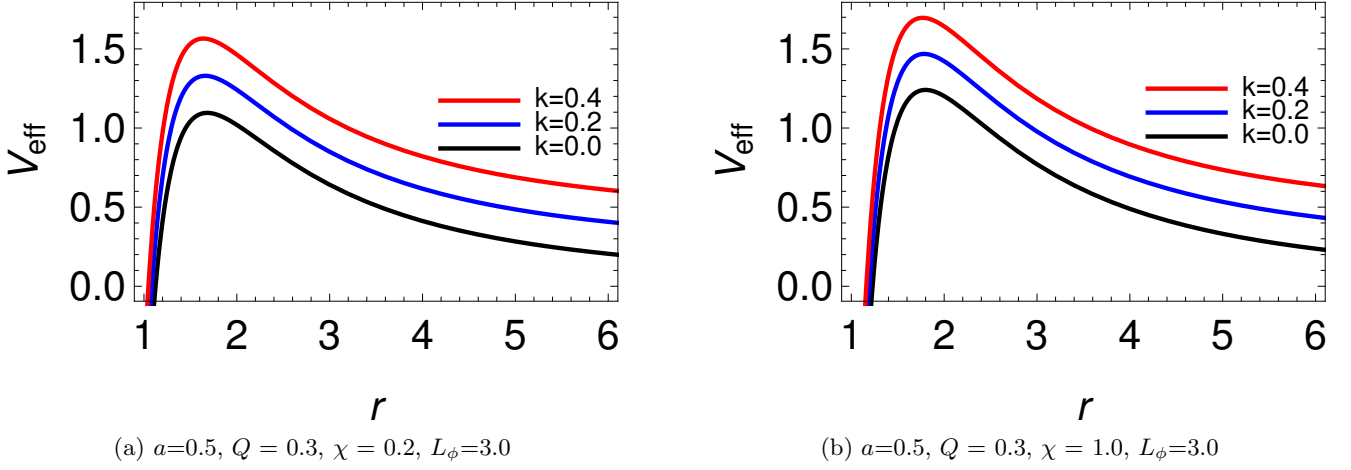


Figure 8: Variation of the effective potential (V_{eff}) with homogenous plasma ($n = constant$).

The above Fig.8 shows the effective potential (V_{eff}) encountered by the photons with variation in plasma parameter k . Here we consider the plasma distribution to be homogenous such that $n = \sqrt{1-k}$. The left one is for $\chi = 0.2$ and the right one for $\chi = 1.0$. The plots are shown by considering $M = 1, E = 1, a = 0.5, Q = 0.3, L_\phi=3.0$. We find that with increase in plasma parameter the potential increases uniformly in both cases. The potential shows a maxima which corresponds to unstable photon orbits. The maxima in case of $\chi = 1.0$ are a little higher than the same for $\chi = 0.2$. Also we find that the position of the maxima, which gives the unstable photon radius (r_p) slightly shifts towards left with increase in plasma parameter k .

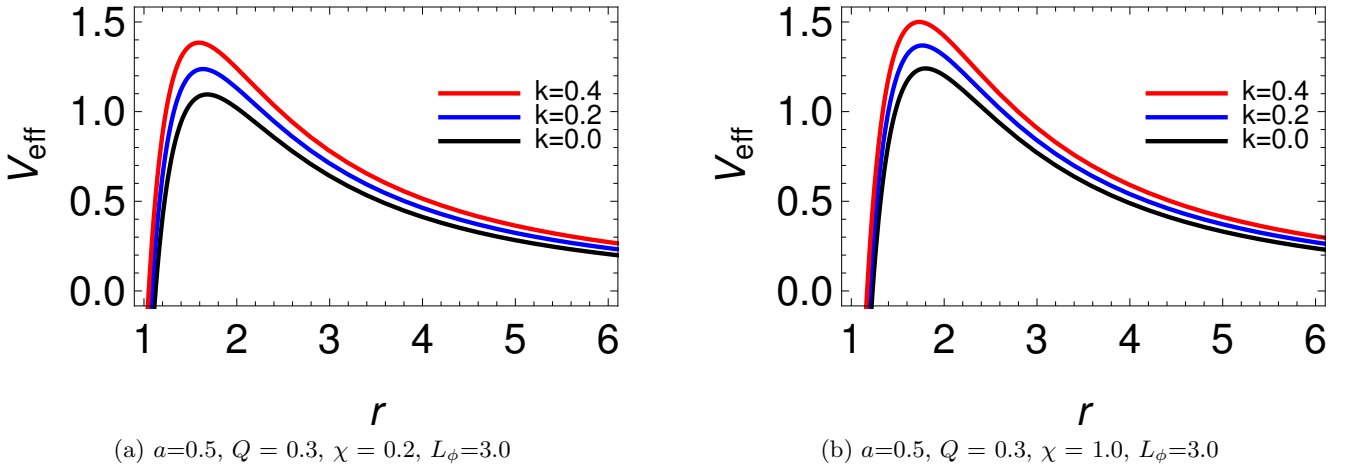


Figure 9: Variation of the effective potential (V_{eff}) with inhomogenous plasma ($n = n(r)$).

Fig.9 shows the effective potential (V_{eff}) faced by the photons with variation in plasma parameter k . The left one is for $\chi = 0.2$ and the right one for $\chi = 1.0$. We consider the plasma distribution to be inhomogenous such that $n(r) = \sqrt{1 - \frac{k}{r}}$. The plots are shown by considering $M = 1, E = 1, a = 0.5, Q = 0.3, L_\phi=3.0$. We find that with increase in plasma parameter (k), the potential increases uniformly in both cases. The potential shows a maxima which corresponds to unstable photon orbits. The maxima in case of $\chi = 1.0$ are a little higher than the same for $\chi = 0.2$. Also we find that the position of the maxima shifts towards left with increase in plasma parameter k . This implies that the radius (r_p) of the unstable photon orbits decreases with increase in plasma parameter k , i.e., the orbits move close to the black hole. The increment of effective potential in both the above cases for homogenous and inhomogenous plasma can be assigned to the fact that the presence of plasma adds up to the mass of the system and thereby the total energy increases. So by radial equation (52) for fixed r , increase in energy increases the potential. Thus the potential of the system increases with increase in plasma parameter k .

7 Summary and conclusion

After running through the analysis in details, we now summarise our results. We consider a charged rotating black hole surrounded by perfect fluid dark matter (*PFDM*). We also immerse the system in plasma and consider no interaction between plasma and dark matter. We have considered radial plasma number distribution in this study.

We observe some unique characteristics of the black hole spacetime due to presence of *PFDM*. From the analysis of the function $\Delta(r)$, we find that the outer event horizon (r_{h+}) decreases with increase in *PFDM* parameter (χ). The decrement proceeds until $\chi < \chi_c$. At this point and beyond, we observe a reverse nature where r_{h+} increases with further increase in χ . The same behaviour gets reflected in the observed black hole shadow. The reason for such a fascinating observation can be assigned to the contribution of *PFDM* to the mass of the black hole system. Here, we have two masses, M for the original black hole and M_0 for the black hole corresponding to *PFDM*. Till $\chi < \chi_c$, the black hole mass is M and gets inhibited by M_0 . But just at the point when $\chi = \chi_c$, the total mass is given by M_0 beyond which system mass increases with increase in χ . Since the mass has a major effect in determining the event horizon of the black hole and thereby the shadow, hence we obtain such results.

Then we move on to analyse the motion of null particles around the black hole. These particles can be rotating along the direction of black hole spin (co-rotating) or opposite (counter rotating) to it. We observed that those co-rotating orbits lie close to the black hole whereas, the counter rotating ones remain away from the black hole. We find their dependence on plasma parameter. The effect of plasma is independent of the influence of dark matter. We find that in case of homogenous plasma distribution ($n = \sqrt{1-k}$), the radius of co-rotating orbits decrease whereas that for the counter rotating orbits increase with increase in plasma parameter k . Also, we find that with increase in plasma parameter (k) in case of inhomogenous plasma distribution ($n = \sqrt{1 - \frac{k}{r}}$), the increase in k results in decrease of photon radius for both co-rotating and counter rotating orbits.

Then we obtain the null geodesics responsible for the formation of the black hole shadow. With the help of the geodesic equation(s), we obtain the celestial coordinates (α, β). These two coordinates give the black hole shadow radius (R_s) as $R_s^2 = \alpha^2 + \beta^2$. The shadow gets formed in the celestial plane ($\alpha - \beta$ plane). We plot the shadow and study the dependence of the black hole shadow on the black hole parameters (a, Q, χ, k). From the plots, we find that the shadow gets rotated and deformed with increase in black hole spin (a). The deformation of black hole shadow occurs due to the rotational drag of the unstable photons by the black hole. We also observe that increment in charge (Q) reduces the radius (R_s) and thereby the size of the black hole shadow. The reason for this is quite obvious. The black hole shadow is the image of the outer event horizon of the black hole. The radius of outer event horizon is given as $r_{h+} = M + \sqrt{M^2 - Q^2}$ in absence of χ and k . With increase in Q , r_{h+} decreases and thereby R_s decreases. This ultimately reduces the size of the black hole shadow.

Next we analyse the effect of the plasma medium on the black hole shadow. The shadow is formed by the light rays encircling the black hole in unstable photon orbits. If these light rays move through vacuum, they have no deviation. But if they move through plasma media, they get deviated due to variation in frequency. The black hole shadow is formed in the celestial plane with coordinates α and β . The extreme right of α axis corresponds to the radius of counter rotating orbits (r_{p2}) whereas that on the extreme left corresponds to the co-rotating orbits (r_{p1}). The variation of the the radius of these orbits with plasma gets reflected in the black hole shadow. Thus the shadow radius (r_p) increase or decrease accordingly in case of homogenous and inhomogenous plasma.

Finally, we have analysed the effective potential (V_{eff}) and have found that it significantly depends on the plasma parameter (k). The maxima of the potential (V_{eff}) corresponds to the radius of the unstable photon orbits. These maxima's shift towards left for both homogenous and inhomogenous plasma distribution. Besides, we also find that the peak of the effective potential increases with increase in plasma parameter k . The reason for such an increment can be related to the fact that plasma adds up to the mass and thereby to the energy of the total system and hence the potential (V_{eff}) of the system increases.

From our analysis we also find that the effects of the black hole parameters, such as spin (a), charge (Q), *PFDM* parameter (χ) and plasma parameter (k) on the black hole shadow are independent of each other.

Acknowledgments

A.D. would like to acknowledge the support of S.N. Bose National Centre for Basic Sciences for Senior Research Fellowship. A.S. acknowledges the financial support by Council of Scientific and Industrial Research (CSIR, Govt. of India).

References

- [1] A. Das, A. Saha and S. Gangopadhyay, *Investigation of the circular geodesics in a rotating charged black hole in presence of perfect fluid dark matter*, *Class. Quantum Grav.* **38** (2021) 6, 065015.
- [2] Event Horizon Telescope Collaboration, *First M87 Event Horizon Telescope Results. I. The Shadow of the Supermassive Black Hole*, *The Astrophysical Journal Letters* **875** (2019) L1.
- [3] J. L. Synge, *The escape of photons from gravitationally intense stars*, *Mon. Not. R. Astron. Soc.* **131** (1966) 463-466.
- [4] J.P. Luminet, *Image of a Spherical black hole with Thin Accretion disk*, *Astron. Astrophys* **75** (1979) 228-235.
- [5] J.M. Bardeen, *Timelike and null geodesics in the Kerr metric*, *Black holes (Les astres occlus)* (1973) 215-239.
- [6] K. Hioki and K.I. Maeda, *Measurement of the Kerr spin parameter by observation of a compact object's shadow*, *Phys. Rev. D* **80** (2009) 024042.
- [7] A de Vries, *The apparent shape of a rotating charged black hole, closed photon orbits and the bifurcation set A_4* , *Class. Quantum Grav.* **17** (2000) 123.
- [8] A. Grenzebach, V. Perlick and C. Lämmerzahl, *Photon regions and shadows of accelerated black holes*, *International Journal of Modern Physics D* **24** (2015) 9, 1542024.
- [9] A. Övgün, İ. Sakallı and J. Saavedraa, *Shadow cast and deflection angle of Kerr-Newman-Kasuya spacetime*, *JCAP* **10** (2018) 041.
- [10] S. W. Wei, Y. C. Zou, Y. X. Liu, R. B. Mann, *Curvature radius and Kerr black hole shadow*, *JCAP* **08** (2019) 030.
- [11] A. Abdujabbarov, M. Amir, B. Ahmedov and S. G. Ghosh, *Shadow of rotating regular black holes*, *Phys. Rev. D* **93** (2016) 104004.
- [12] M. Wang, S. Chen, J. Jing, *Shadow casted by a Konoplya-Zhidenko rotating non-Kerr black hole*, *JCAP* **10** (2017) 051.
- [13] A. K. Mishra, S. Chakraborty, S. Sarkar, *Understanding photon sphere and black hole shadow in dynamically evolving spacetimes*, *Phys. Rev. D* **99** (2019) 104080.
- [14] R. Kumar, B. P. Singh, S. G. Ghosh, *Shadow and deflection angle of rotating black hole in asymptotically safe gravity*, *Annals Phys.* **120** (2020) 168252.
- [15] R. A. Hennigar, M. B. J. Poshteh, and R. B. Mann, *Shadows, signals, and stability in Einsteinian cubic gravity*, *Phys. Rev. D* **97** (2018) 064041.
- [16] H. Khodabakhshi, A. Giaimo, R. B. Mann, *Einstein Quartic Gravity: Shadows, Signals, and Stability*, *Phys. Rev. D* **102** (2020) 044038.
- [17] M. Amir, S. G. Ghosh, *Shapes of rotating nonsingular black hole shadows*, *Phys. Rev. D* **94** (2016) 024054.

- [18] R. Shaikh, *Black hole shadow in a general rotating spacetime obtained through Newman-Janis algorithm*, *Phys. Rev. D* **100** (2019) 024028.
- [19] E. Contreras, Á. Rincón, G. Panotopoulos, P. Bargueño, and B. Koch, *Black hole shadow of a rotating scale-dependent black hole*, *Phys. Rev. D* **101** (2020) 064053.
- [20] H. Lü and H. D. Lyu, *Schwarzschild black holes have the largest size*, *Phys. Rev. D* **101** (2020) 044059.
- [21] X. H. Feng, H. Lü, *On the size of rotating black holes*, *Eur. Phys. J. C* **80** (2020) 551.
- [22] R. Kumar, S. G. Ghosh, and A. Wang, *Gravitational deflection of light and shadow cast by rotating Kalb-Ramond black holes*, *Phys. Rev. D* **101** (2020) 104001.
- [23] L. Ma, H. Lü, *Bounds on photon spheres and shadows of charged black holes in Einstein-Gauss-Bonnet-Maxwell gravity*, *Phys. Letters B* **807** (2020) 135535.
- [24] R. A. Konoplya and A. Zhidenko, *Analytical representation for metrics of scalarized Einstein-Maxwell black holes and their shadows*, *Phys. Rev. D* **100** (2019) 044015.
- [25] R. Kumar, S. G. Ghosh, and A. Wang, *Shadow cast and deflection of light by charged rotating regular black holes*, *Phys. Rev. D* **100** (2019) 124024.
- [26] S. Dastan, R. Saffari, S. Soroushfar, *Shadow of a Kerr-Sen dilaton-axion Black Hole*, arXiv:1610.09477 [gr-qc].
- [27] A. Das, A. Saha, S. Gangopadhyay, *Shadow of charged black holes in Gauss-Bonnet gravity*, *Eur.Phys.J.C* **80** (2020) 3, 180.
- [28] A. Saha, S. M. Modumudi, S. Gangopadhyay, *Shadow of a noncommutative geometry inspired Ayón Beato García black hole*, *Gen.Rel.Grav.* **50** (2018) 8, 103.
- [29] L. Amarilla, E. F. Eiroa, *Shadow of a rotating braneworld black hole*, *Phys. Rev. D* **85** (2012) 064019.
- [30] L. Amarilla, E. F. Eiroa, *Shadow of a Kaluza-Klein rotating dilaton black hole*, *Phys. Rev. D* **87** (2013) 044057.
- [31] A. Grenzebach, V. Perlick, C. Lämmerzahl, *Photon Regions and Shadows of Kerr-Newman-NUT Black Holes with a Cosmological Constant*, *Phys. Rev. D* **89** (2014) 124004.
- [32] L. Amarilla, E. F. Eiroa, G. Giribet, *Null geodesics and shadow of a rotating black hole in extended Chern-Simons modified gravity*, *Phys. Rev. D* **81** (2010) 124045.
- [33] S. Dastan, R. Saffari, S. Soroushfar, *Shadow of a Charged Rotating Black Hole in $f(R)$ Gravity*, arXiv:1606.06994 [gr-qc].
- [34] R. Kumar, B. P. Singh, Md. S. Ali, S. G. Ghosh, *Rotating black hole shadow in Rastall theory*, arXiv:1712.09793 [gr-qc].
- [35] T. Vetsov, G. Gyulchev, S. Yazadjiev, *Shadows of Black Holes in Vector-Tensor Galileons Modified Gravity*, arXiv:1801.04592 [gr-qc].
- [36] H. M. Wang, Y. M. Xu, S. W. Wei, *Shadows of Kerr-like black holes in a modified gravity theory*, *JCAP* **03** (2019) 046.
- [37] T. Zhu, Q. Wu, M. Jamil, K. Jusufi, *Shadows and deflection angle of charged and slowly rotating black holes in Einstein-Æther theory*, *Phys. Rev. D* **100** (2019) 044055.
- [38] A. Övgün, İ. Sakalli, J. Saavedra and C. Leiva, *Shadow cast of noncommutative black holes in Rastall gravity*, *Modern Phys. Letters A* **35** (2020) 20, 2050163.

- [39] U. Papnoi, F. Atamurotov, S. G. Ghosh, B. Ahmedov, *Shadow of five-dimensional rotating Myers-Perry black hole*, *Phys. Rev. D* **90** (2014) 024073.
- [40] A. Abdujabbarov, F. Atamurotov, N. Dadhich, B. Ahmedov, Z. Stuchlík *Energetics and optical properties of 6-dimensional rotating black hole in pure Gauss-Bonnet gravity*, *Eur. Phys. J. C* **75** (2015) 399.
- [41] B. P. Singh, S. G. Ghosh, *Shadow of Schwarzschild–Tangherlini black holes*, *Annals of Physics* **395** (2018) 127-137.
- [42] V. Perlick, O. Yu. Tsupko, G. S. Bisnovaty-Kogan, *Black hole shadow in an expanding universe with a cosmological constant*, *Phys. Rev. D* **97** (2018) 104062.
- [43] P. C. Li, M. Guo, B. Chen, *Shadow of a Spinning Black Hole in an Expanding Universe*, *Phys. Rev. D* **101** (2020) 084041.
- [44] P. J. E. Peebles and B. Ratra, *The cosmological constant and dark energy*, *Rev. Mod. Phys* **75** (2003) 559.
- [45] K. Koyama, *The cosmological constant and dark energy in braneworlds*, *Gen Relativ Gravit* **40** (2007) 421-450.
- [46] J. Zhang, X. Zhang, H. Liu, *Agegraphic dark energy as a quintessence*, *Eur. Phys. J. C* **54** (2008) 303-309.
- [47] S. Tsujikawa, *Quintessence: a review*, *Class. Quantum Grav.* **30** (2013) 214003.
- [48] V. C. Rubin, Jr. W. K. Ford, and N. Thonnard, *Rotational properties of 21 SC galaxies with a large range of luminosities and radii, from NGC 4605 ($R=4kpc$) to UGC 2885 ($R=122kpc$)*, *Astro. Phys. J.* **238** (1980) 471.
- [49] F. Zwicky, *The redshift of extragalactic nebulae*, *Helv. Phys.Acta.* **6** (1933) 110.
- [50] V. V. Kiselev, *Quintessence and black holes*, *Class. Quantum Grav.* **20** (2003) 6, 1187.
- [51] V. V. Kiselev, *Quintessential solution of dark matter rotation curves and its simulation by extra dimensions*, arXiv: 0303031 [gr-qc].
- [52] M. H. Li, K. C. Yang, *Galactic dark matter in the phantom field*, *Class. Quantum Grav.* **86** (2012) 123015.
- [53] Y. Heyderzade and F. Darabi, *Black hole solutions surrounded by perfect fluid in Rastall theory*, *Phys. Letts. B* **771** (2017) 365-373.
- [54] Z. Xu, X. Hou, J. Wang, *Kerr-anti-de Sitter/de Sitter black hole in perfect fluid dark matter background*, *Class. Quantum Grav.* **35** (2018) 115003.
- [55] Z. Xu, X. Hou, J. Wang, Y. Liao, *Perfect Fluid Dark Matter Influence on Thermodynamics and Phase Transition for a Reissner-Nordstrom-Anti-de Sitter Black Hole*, *Adv. in High Energy Phys.* (2019) 2434390.
- [56] S. Haroon, M. Jamil, K. Jusufi, K. Lin and R. B. Mann, *Shadow and deflection angle of rotating black holes in perfect fluid dark matter with a cosmological constant*, *Phys. Rev. D* **99** (2019) 044015.
- [57] H. X. Zhang, Y. Chen, P. Z. He, Q. Q. Fan, and J. B. Deng, *Bardeen black hole surrounded by perfect fluid dark matter*, arXiv:2007.09408v1 [gr-qc].
- [58] X. Hou, Z. Xu, J. Wang, *Rotating black hole shadow in perfect fluid dark matter*, *JCAP* **12** (2018) 040.

- [59] V. Perlick and O. Yu. Tsupko, *Calculating black hole shadows: review of analytical studies*, arXiv:2105.07101 [gr-qc].
- [60] V. Perlick, O. Yu. Tsupko, and G. S. Bisnovaty-Kogan, *Influence of a plasma on the shadow of a spherically symmetric black hole*, *Phys. Rev. D* **92** (2015) 104031.
- [61] F. Atamurotov, B. Ahmedov, and A. Abdujabbarov, *Optical properties of black holes in the presence of a plasma: The shadow*, *Phys. Rev. D* **92** (2015) 084005.
- [62] M. Sharif, S. Iftikhar, *Shadow of a charged rotating non-commutative black hole*, *Eur. Phys. J. C* **76** (2016) 630.
- [63] V. Perlick, O. Yu. Tsupko, *Light propagation in a plasma on Kerr spacetime: Separation of the Hamilton-Jacobi equation and calculation of the shadow*, *Phys. Rev. D* **95** (2017) 104003.
- [64] G. S. Bisnovaty-Kogan, O. Yu. Tsupko, *Gravitational Lensing in Presence of Plasma: Strong Lens Systems*, *Black Hole Lensing and Shadow*, *Universe* **3** (2017) 3, 57.
- [65] A. Abdujabbarov, B. Toshmatov, Z. Stuchlík and B. Ahmedov, *Shadow of the rotating black hole with quintessential energy in the presence of plasma*, *IJMPD* **26** (2017) 6, 1750051.
- [66] Y. Huang, Y. P. Dong and D. J. Liu, *Revisiting the shadow of a black hole in the presence of a plasma*, *IJMPD* **27** (2018) 12, 1850114.
- [67] B. Ahmedov, B. Turimov, Z. Stuchlík and A. Tursunov, *Optical properties of magnetized black hole in plasma*, *IJMPD: Conference Series* **49** (2019) 1960018.
- [68] G. Z. Babar, A. Z. Babar, F. Atamurotov, *Optical properties of Kerr–Newman spacetime in the presence of plasma*, *Eur. Phys. J. C* **80** (2020) 761.
- [69] A. Chowdhuri, A. Bhattacharyya, *Shadow analysis for rotating black holes in the presence of plasma for an expanding universe*, *Phys. Rev. D* **104** (2021) 064039.
- [70] C. Q. Liu, C. K. Ding, J. L. Jing, *Effects of Homogeneous Plasma on Strong Gravitational Lensing of Kerr Black Holes*, *Chin. Phys. Lett.* **34** (2017) 9, 090401.
- [71] R. A. Breuer, J. Ehlers, *Propagation of electromagnetic waves through magnetized plasmas in arbitrary gravitational fields*, *Astron. Astrophys.* **96** (1981) 1-2, 293-295.
- [72] V. Perlick, *Ray Optics, Fermat's Principle, and Applications to General Relativity*, (Springer, Berlin, 2000).
- [73] J. L. Synge, *Relativity. The General Theory*, (North-Holland, Amsterdam, 1960).
- [74] A. Rogers, *Frequency-dependent effects of gravitational lensing within plasma*, *Mon. Not. Royal Astron. Soc.* **451** (2015) 1, 17-25.
- [75] S. Chandrasekhar, *The Mathematical Theory of Black Holes*, Oxford University Press, Oxford (1998).
- [76] R. Shaikh, K. Pal, K. Pal and T. Sarkar, *Constraining alternatives to the Kerr black hole*, *Mon. Not. Royal Astron. Soc.* **506** (2021), 1229–1236.